Ionics (2023) 29:2405–2415
https://doi.org/10.1007/s11581-023-04991-3

ORIGINAL PAPER

Highly active and durable hollow NiPt/C as electrocatalysts for methanol electro-oxidation reaction

Jia-Jun Han[1] · **Ming-yu Yin**[1]

Received: 10 January 2023 / Accepted: 5 April 2023 / Published online: 20 April 2023

Abstract

At present, platinum-based alloys are irreplaceable catalysts for direct methanol fuel cells. How to reduce the amount of Pt and improve its electrocatalytic performance is one of the difficulties in this field. Noble-metal hollow nanocrystals are one of the most promising catalysts due to their high specific surface area and high stability. In this paper, we used the combination of electrochemical displacement reaction and Kirkendal effect to prepare hollow NiPt/C by sacrificial template method, and explore the effect of capping agent content on the electrocatalytic methanol oxidation reaction (MOR) performance of synthetic materials. Electrochemical tests show that the hollow binary catalyst prepared with a capping agent content of 50 mg had the highest electrochemical active area. In particular, 4000-s chronoamperometry tests in acidic solution show that the stability of NiPt/C with hollow structure is enhanced. We ascribe the better catalytic activity to the hollow feature, higher specific electrochemical surface area, and more abundant active sites.

Keywords Methanol oxidation · Platinum nanoparticles · Electrocatalysts · Hollow

Introduction

Precious metals and their alloys have been widely used in proton exchange membrane fuel cells, including direct methanol fuel cells, due to their high electrocatalytic performance [1, 2]. However, the high price of precious metals has become one of the important factors restricting costs [2]. At present, there are two feasible ways to reduce catalyst cost: one is to improve the utilization of precious metals in the catalyst, the other is to develop non-precious metal catalysts [3, 4]. Long and extensive work has been carried out on the search for non-noble metal catalysts. However, research shows that there is still a large gap between the electrocatalytic activity of non-noble metal catalysts and that of noble metal catalysts [1, 5–7]. Therefore, noble metal catalysts, especially platinum-based alloys, are still the most promising electrocatalytic materials and can meet the needs of direct methanol fuel cells [8–12].

It is well known that traditional single-metal Pt catalysts are vulnerable to the toxicity of CO generated in the indirect path of MOR process or CO like intermediates, leading to a serious decline in reaction kinetics. Therefore, it is an urgent problem to develop a reasonable strategy to improve CO tolerance and increase the number of active sites of Pt-based polymetallic catalysts. Platinum-based binary nanomaterials have received extensive attention and research due to their special physical and chemical structures, adjustable element compositions, and synergistic effects [13–15]. Alloying Pt with cheap metals, especially 3d transition metals, can change the electronic configuration of Pt and weaken the interaction between Pt and Pt-OH intermediates, thus enhancing its catalytic performance [16]. Huang [17] presents a convenient and cost-effective approach to the stereoassembly of quasi-one-dimensional grain boundary-enriched Pt nanoworms on nitrogen-doped low-defect graphitic carbon nanosheets. Benefiting from its numerous catalytically active grain boundaries as well as optimized electronic structure, the as-derived Pt NWs/NL-CNS catalyst possesses exceptionally good electrocatalytic properties for methanol oxidation.

Up to now, many PtM (M = Cu [18], Fe [19, 20], Co [8, 10], Ni [21], etc.) general-purpose Pt-based binary catalysts have been studied to improve catalytic activity and stability and reduce the use of Pt. It has been pointed out that the (111) crystal surface of Pt_3Ni alloy formed by transition metal Ni and Pt

✉ Jia-Jun Han
hanjiajunhitweihai@163.com

[1] School of Marine Science and Technology, Harbin Institute of Technology, Weihai 264209, China

shows extremely high ORR electrocatalytic activity, which is 10 times higher than that of single metal Pt (111) crystal surface under the same conditions, and 90 times higher than that of commercial Pt/C catalyst [22, 23]. The analysis shows that the Pt_3Ni surface has a special d-band electronic structure and the phenomenon of surface atom rearrangement, which leads to the weakening of its adsorption capacity for oxygen-containing species that do not participate in the reaction in the system, and the increase of active sites for O_2 adsorption on the side [22].

In addition to the influence of components, the catalytic activity of nanostructured Pt-based catalysts is highly dependent on their surface area, surface atomic structure, crystal size, and shape. By controlling the size and shape of the catalyst, large surface area and rich catalytic active sites can be obtained. Therefore, the structure of platinum alloy nanocatalysts has become a key research direction. Pt alloy nanocatalyst [16], M@Pt [24, 25], Pt monolayer [26, 27], heterojunction catalyst [28], and hollow Pt [3] are widely used to improve the utilization rate of Pt in catalyst. The hollow porous structure has obvious advantages. The reasons are as follows: (1) The nanomaterials with hollow porous structure have high comparative area and pore volume. (2) The regulation of the structural parameters (thickness, porosity, surface derivatization, etc.) of the "shell" of the hollow nanomaterials can adapt to a variety of catalytic needs. (3) Homogeneous hollow nanomaterials are not easy to be affected by Ostwald ripening. Nanoparticles are not easy to dissolve and agglomerate in the process of catalytic reaction, so they show higher stability.

Wang's team [29, 30] has synthesized various components, sizes, and shapes of NiPt nanospheres with smooth shells. Compared with commercially available Pt/C, the prepared hollow products showed enhanced electrocatalytic performance for the oxidation of methanol and ethylene glycol. Wu [31] et al. synthesized a new graphene supported hollow PtNi nanocatalyst by the current displacement method at ambient temperature, and proved that the morphology and size of the prepared nanocatalyst have a great relationship with the type of capping agent, and the stability effect of PVP is far better than that of CTAB and SDS.

In this study, using self-made Ni nanospheres as sacrificial templates, XC-72 loaded hollow NiPt nanomaterials were successfully prepared by using the Kirkendall effect at the nanoscale in aqueous solution, and the electrocatalytic properties of the nanomaterials synthesized under different concentrations of PVP were compared.

Experimental

Materials

Nickel (II) chloride anhydrous ($NiCl_2$), chloroplatinic acid (H_2PtCl_6), methanol (CH_3OH), and ethanol absolute (CH_3CH_2OH) were purchased from Aladdin. Poly(vinylpyrrolidone) (PVP; MW = 30,000 g/mol) and sodium borohydride ($NaBH_4$, 98%) were purchased from Sinopharm Chemical Reagent Co. Ltd. Vulcan XC-72R carbon was obtained from E-TEK. All reagents were used without further purification.

Synthesis of binary hollow NiPt/C

First, add 0.85 mL 10 g/L of nickel chloride standard solution and some (20 mg, 35 mg, 50 mg, 65 mg, and 80 mg) PVP to 20 mL of ultrapure water, and make it completely dissolved after ultrasonic dispersion treatment at room temperature for 15 min. Fill the solution with high-purity nitrogen for 15 min continuously to remove dissolved oxygen in the solution. Then, weigh 5 mg of sodium borohydride and dissolve it in 5 mL of ultrapure water. Use a rubber tip dropper to drop this solution into the precursor solution at a uniform speed, and perform rapid magnetic stirring. During this process, it can be observed that the color of the solution quickly changes to dark brown, which means that the Ni template has been prepared. Then, reduce the stirring rate, slowly drop 1.84 mL of 39 mM H_2PtCl_6 solution into the dispersion, and continue stirring for 2 h. Then, 55.8 mg XC-72 was added to the solution and stirred continuously for 1 h. Nitrogen was continuously injected into the reaction system throughout the process. Finally, the newly prepared sample was filtered with water and ethanol and dried at 55 ℃ to obtain the binary catalytic material NiPt/C with different PVP dosages.

Structural and morphological characterization

The morphology of hollow NiPt/C was characterized by transmission electron microscopy (TEM) (Tecnai G2 F20) (DX 2700).

X-ray diffraction (XRD) patterns were obtained using a DX-2700 diffractometer (Dandong Haoyuan, China), irradiated with Cu-Kα ($\lambda = 1.5425$ Å), and scanned from 0° to 90°.

The surface composition and electronic structure of the samples were characterized by X-ray photoelectron spectroscopy (XPS, Thermo Fisher).

Fabrication of the working electrode for half-cell measurement

The catalyst ink was prepared by dispersing 4 mg of catalyst in a mixture of 0.375 mL ultra-pure water, 0.125 mL anhydrous ethanol, and 50 µL of 5 wt% Nafion solution. Then, add 5 µL ink that is cast on the glass carbon electrode (GCE) with a diameter of 3 mm. The GCE is polished with alumina powder with particle size of 50 nm before use.

The electrochemical properties of each catalyst in this paper were tested at Shanghai Chenhua Electrochemical Workstation (CHI660E). The test system was a standard

three-electrode system, with platinum wire electrode as the counter electrode, saturated calomel electrode (SCE) as the reference electrode, and glassy carbon electrode as the working electrode.

The electrochemical surface area measurements

The cyclic voltammograms were conducted in a 0.5 M H_2SO_4 solution within the potential range of − 0.241 ~ 0.959 V(vs.SCE) at the scan rate of 50 mV·s^{-1}. The electrochemical surface area (ECSA) of platinum of the synthesized hollow NiPt/C and the commercial Pt/C was calculated based on the coulombic charges associated with hydrogen adsorption and desorption in the hydrogen region (0.241 ~ 0.959 V) after deducting the double-layer charging current [32].

$$ECSA = Q_H/\left(0.21 \times M_{Pt}\right) \quad (1\text{-}1)$$

where Q_H (mC) is the charge due to hydrogen adsorption/desorption in the hydrogen region of the CVs, 0.21 mC·cm^{-2} is the electrical charge associated with the monolayer adsorption of hydrogen on Pt, and M_{Pt} is the loading of Pt metal on the working electrode.

Methanol oxidation reaction

The electrocatalytic oxidation of methanol was carried out in a 0.5 M H_2SO_4 solution with 0.5 M to the methanol concentrations within the potential from − 0.241 to 0.959 V at the scan rate of 50 mV·s^{-1}. Prior measurements, the solution was purged with high-purity nitrogen for at least 30 min, and a nitrogen environment was maintained over the solution to prevent the solution from oxygen.

The catalytic stability of the nanocatalyst was evaluated by amperometry under an applied potential of 0.4 V (vs. SCE). In addition, commercial Pt/C catalyst and hollow catalyst were tested for 250 cycles of cyclic voltammetry to compare their CO poisoning resistance.

Results and discussion

Structural and morphological characterization

Figure 1 is an electron microscope photo of hollow nanospheres synthesized by metal exchange method. It can be clearly seen from the figure that the middle part of the nanospheres is brighter than the edge part, indicating that the middle part is empty and the edge is a shell. These hollow nanospheres have good dispersion and no obvious agglomeration. This structure enables the nanoparticles to have a larger specific surface area, which can provide more active reaction sites in the electrocatalytic oxidation of methanol. XC-72 supported Pt-Ni nanocatalyst can be synthesized by electrodisplacement reaction with $PtCl_6^{2-}$ and Ni^{2+} as precursors. $NaBH_4$ reduces Ni^{2+} to Ni. After adding $PtCl_6^{2-}$, hollow Pt–Ni nanostructures are formed due to the displacement reaction between Ni nanospheres and $PtCl_6^{2-}$.

The structure and morphology of hollow NiPt/C catalyst were characterized by TEM (Fig. 1a, b). The image recorded at a lower magnification shows that the middle part of the nanosphere is obviously brighter than its edge part, indicating that the middle part is empty and the edge is a shell. TEM images at higher magnification show that the thickness of the shell is about 20 nm, and the shell seems rough, consisting of many Pt–Ni nanoparticles with a size of 1 ~ 2 nm (Fig. 1b). HR-TEM image (Fig. 1c, d) of nanocatalyst shows the main formation of face-centered cubic (fcc) (111) lattice image, which is slightly smaller than the (111) plane of Pt (0.230 nm) [33], because the lattice shrinks when Pt atoms are replaced by Ni atoms, which confirms the formation of Pt–Ni alloy.

The elemental distribution of Pt, Ni, and C is shown in Fig. 1(e–h). The Pt elements that constitute a hollow NiPt/C sphere are uniformly distributed throughout the entire shell, while Ni elements appear more frequently within the interior of the hollow sphere. Figure 1 (i–j) shows the element content in the interior and outer shells of the hollow sphere. It can be seen that the Pt mass fraction in the outer shell is 87.39%, which is higher than the Pt content in the interior (85.68%), indicating that the outer shell of the hollow sphere is rich in Pt. Combining the characterization of the high-power transmission microscope, it can be fully explained that the catalyst prepared is a hollow sphere, mainly containing two metal elements, Pt and Ni. Moreover, the hollow sphere has a rough shell and a high specific surface area, which can theoretically provide more active sites for methanol catalytic oxidation.

It can be observed from the Fig. 2 that five diffraction peaks are located at 2 θ = 40.0°, 46.5°, 67.9°, and 81.8°, and PtNi(111), (200), (220), and (310) crystal planes with face-centered cubic structure are respectively attributed, which is consistent with the results of selected area electron diffraction in TEM characterization. The wider diffraction peak of hollow NiPt/C sample indicates that the grain size of the hollow catalyst surface is smaller than that of the solid catalyst surface. It is speculated that the hollow NiPt/C sample has a larger specific surface area. Compared with the standard diffraction peak card of Pt (Pt PDF#01–1194), it can be found that the diffraction peaks of hollow NiPt/C samples shift to a high angle, indicating that Ni with smaller atomic radius enters into the lattice of Pt, resulting in the distortion and contraction of the

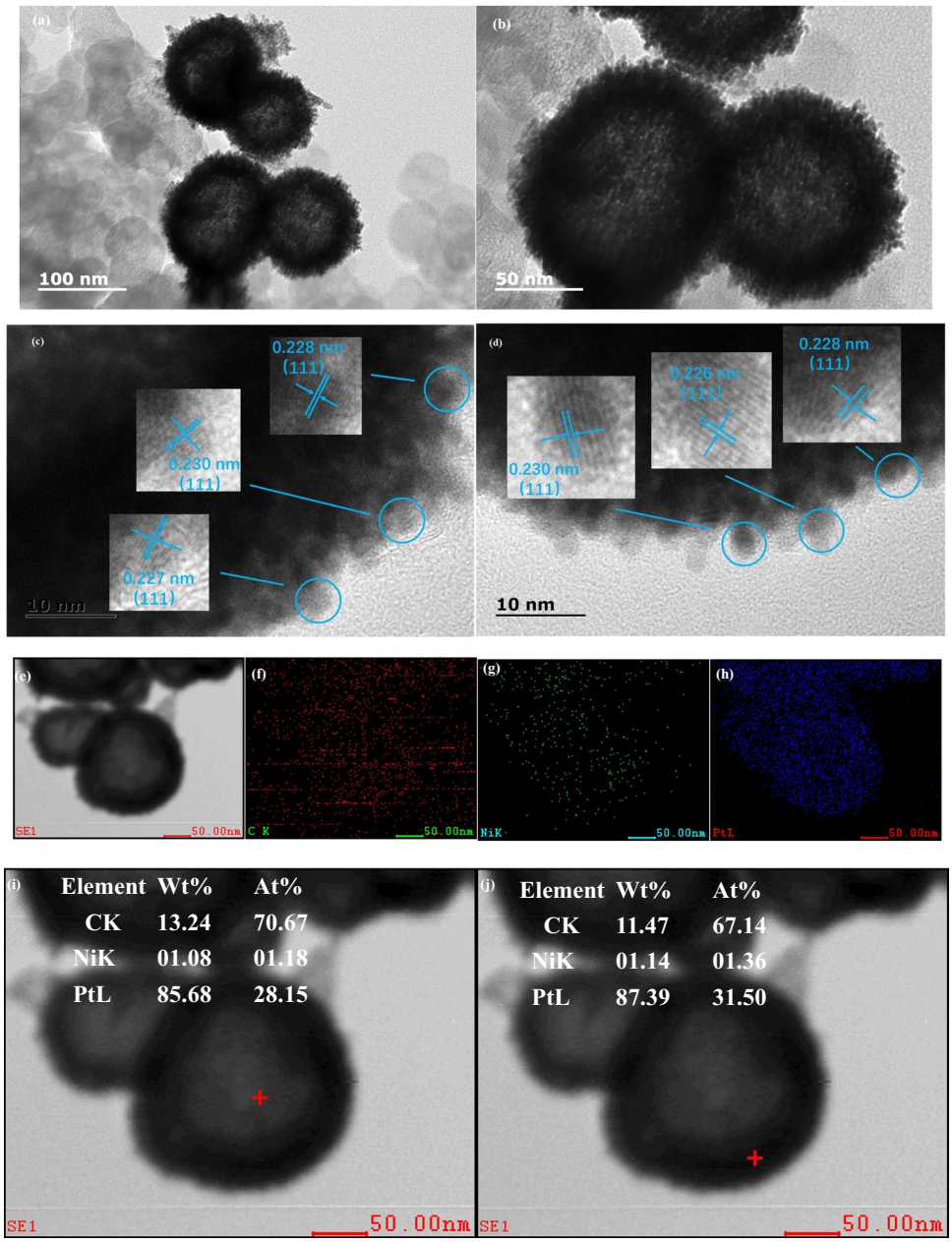

Fig. 1 TEM images of hollow NiPt/C (**a**, **b**); HR-TEM images (**c**, **d**); TEM photographs of a single hollow sphere and corresponding surface scans of C (red), Ni (green), and Pt blue elements (**e**, **f**, **g**, **h**); element content inside and on the surface of a single hollow sphere (**i**, **j**)

lattice of Pt, that is, Pt and Ni in hollow NiPt/C form alloy phases, and no other new phases are formed, which is consistent with the TEM observation results.

Electrochemical characterization

Due to the high specific surface area and high surface energy of nanomaterials, aggregation is prone to occur. Surfactants have amphiphilic properties and can adsorb on the surface of nanoparticles, preventing the aggregation of nanoparticles through the steric hindrance effect of long molecular chains. PVP (K30) is widely used as a water-soluble polymer in the synthesis of hollow nanoparticles. By changing the free energy of the crystal surface, it can change the growth rate of the crystal surface, thereby affecting the morphology of crystal products. PVP can form micelles in solution as a microreactor, limiting the growth of hollow NiPt/C while preventing the aggregation of nanoparticles due to Oswald aging.

When the concentration of PVP in the reaction system is too low to reach the critical micelle concentration, the Oswald phenomenon in the solution system is obvious, and small nanoparticles dissolve and accumulate on the surface of large nanoparticles, making it impossible to prepare hollow spheres. When the amount of PVP input is increased, regular spherical nanoparticles are gradually generated.

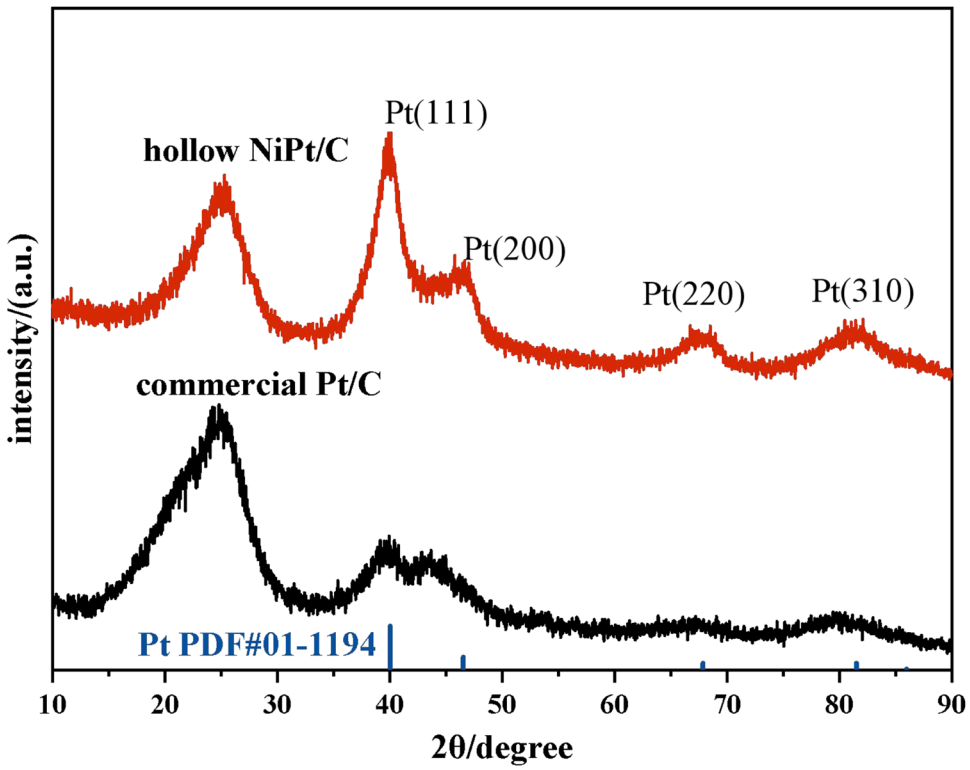

Fig. 2 The XRD patterns of hollow NiPt/C (red line) and Pt/C commercial (black line)

When the PVP in the solution reaches the critical micelle concentration, the long tail end of the active agent forms a steric barrier on the surface of Ni nanoparticles, preventing the aggregation of nanoparticles. When PVP is excessive, it leads to the formation of a large number of irregular nanoparticles, which destroys the stable morphology of nanoparticles.

Figure 3 shows the cyclic voltammetric curve of the catalyst synthesized under different PVP dosages in an acidic medium. Hollow NiPt/C-20 means that the dosage of 20 mg PVP is used in the preparation of catalyst, and the rest is the same. The redox peak at the potential of − 0.241 ~ 0.959 V (vs. SCE) corresponds to the adsorption and desorption of hydrogen, 0.1 ~ 0.3 V (vs. SCE) corresponds to the charge discharge process of double electric layers, and 0.3 ~ 0.959 V (vs. SCE) corresponds to the adsorption and desorption of oxygen [34]. Hydrogen dissociation adsorption peaks appeared in the potential region of − 0.241 ~ 0.959 V (vs. SCE). The peak current of the redox peak of hydrogen dissociation adsorption of hollow NiPt/C-50 was the highest. During the reverse scanning process, a large current peak appeared on the catalyst hollow NiPt/C-50 near 0.4 V, indicating that the catalyst surface synthesized at 50-mg PVP dosage had the weakest chemical adsorption capacity for oxygen-containing species, which was conducive to the oxidative desorption of intermediate products and the release of catalytic active sites.

Figure 4 shows the catalytic activity of MOR electrocatalyst considering the geometric area of the glassy carbon electrode (0.07065 cm^2). The initial oxidation potential of methanol is about 0.2 V (vs. SCE). When the potential is positive scanning, the maximum current peak of methanol oxidation appears at about 0.7 V (vs. SCE). When the

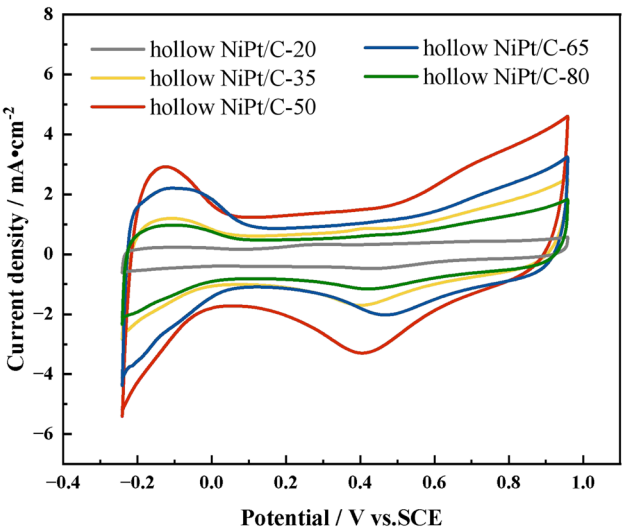

Fig. 3 Cyclic voltammetry results of hollow NiPt/C-20, hollow NiPt/C-35, hollow NiPt/C-50, hollow NiPt/C-65, and hollow NiPt/C-80.CV curves in 0.5 M H_2SO_4. Scan rate 50 mV·$s.^{-1}$ in nitrogen atmosphere at room temperature (RT)

potential is negative scanning, an oxidation current peak also appears at about 0.4 V (vs. SCE). This peak is due to the further oxidation of the incompletely oxidized carbon generated during the positive scanning. Therefore, the ratio I_f/I_b of the positive scan peak current density peak I_f and the negative scan current density peak I_b can be used to characterize the anti-CO performance of the catalyst. The low I_f/I_b ratio indicates that during the positive scan process of methanol oxidation, the excess carbon containing oxides accumulate on the catalyst surface, the worse the anti-poisoning ability of the catalyst is, the opposite is true for the high I_f/I_b ratio, and the stronger the anti-poisoning ability is. The ratio of positive to negative scanning peak current density shows that the I_f/I_b of hollow NiPt/C-50 is 1.9, which is higher than that of other catalysts, indicating that it has better CO poisoning resistance.

It can be seen from Fig. 5 that between 0.15 and 0.25 V (vs. SCE), the current on the scan curve of methanol oxidation begins to increase, which indicates that methanol starts to oxidize, and the corresponding potential is the initial potential of methanol oxidation. The lower the potential or the shift towards the negative potential, the better the catalytic performance of the catalyst. It can be seen from the figure that under a fixed current density (1 mA·cm^{-2}), the catalytic potential of hollow NiPt /C-50 for methanol oxidation is the lowest, indicating that hollow NiPt/C-50 catalyst has the highest catalytic activity.

In order to investigate the stability of the catalyst, the change of methanol oxidation current with time was observed under potentiostatic polarization. Apply a constant potential of 0.4 V (vs. SCE) to the working electrode. Figure 6 shows the polarization current time curves of three types of catalysts for methanol oxidation. It can be clearly seen from the image that during the first 1000 s, the current of all catalysts decayed rapidly, and then gradually became flat. The initial current density (7 mA·cm^{-2}) of hollow NiPt/C-50 is not only higher than that of other catalysts, but also the current decay curve is always above other catalysts, indicating that hollow NiPt/C-50 has more excellent resistance to CO poisoning, and is not easy to be inactivated by methanol in practical applications. This also corresponds to the previous cyclic voltammetry test results.

According to the above experimental results, when the amount of PVP is 50 mg, hollow NiPt/C-50 with stable morphology can be synthesized at room temperature (25 ℃), and has good catalytic activity and anti-CO poisoning ability. This may be due to the fact that the amount of PVP added at 50 mg will make the synthesized Ni nanoparticle template have uniform morphology and no obvious agglomeration, so the size distribution of the synthesized hollow material is narrow and more active sites are exposed. In order to further prove the high performance of the prepared catalyst, it is necessary to compare it with commercial Pt/C.

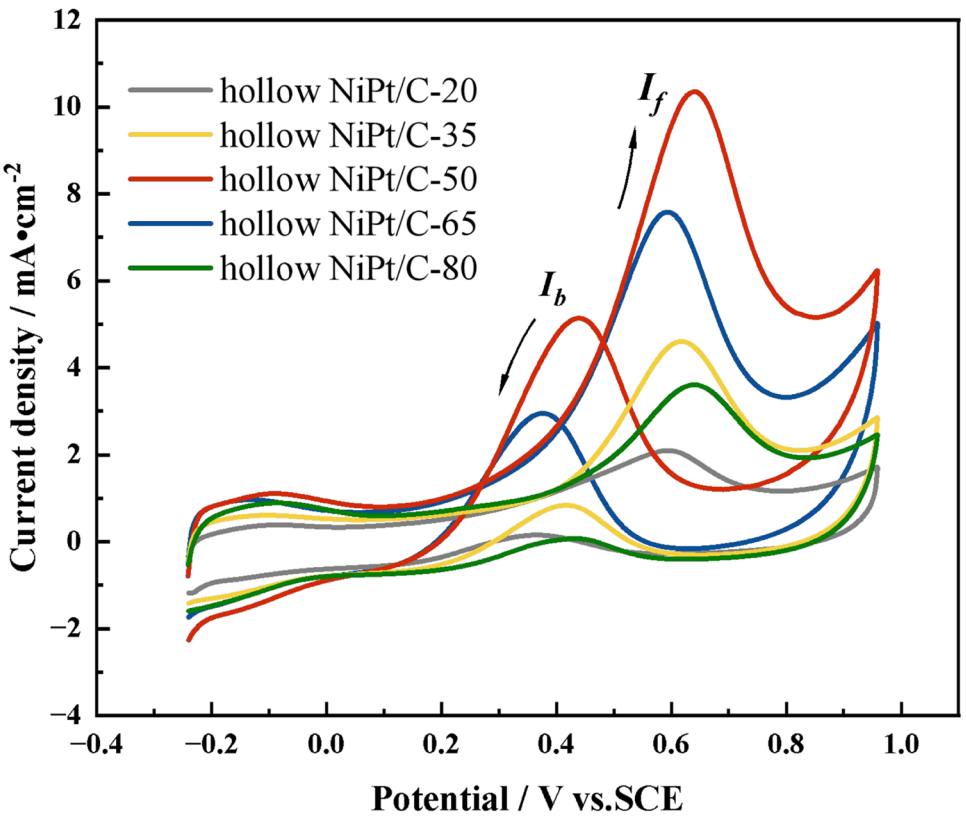

Fig. 4 Geometric MOR curve results of hollow NiPt/C-20, hollow NiPt/C-35, hollow NiPt/C-50, hollow NiPt/C-65, and hollow NiPt/C-80. MOR curves were tested in 0.5 M H_2SO_4 and 0.5 M CH_3OH. Scan rate 50 mV·s^{-1} in nitrogen atmosphere at RT

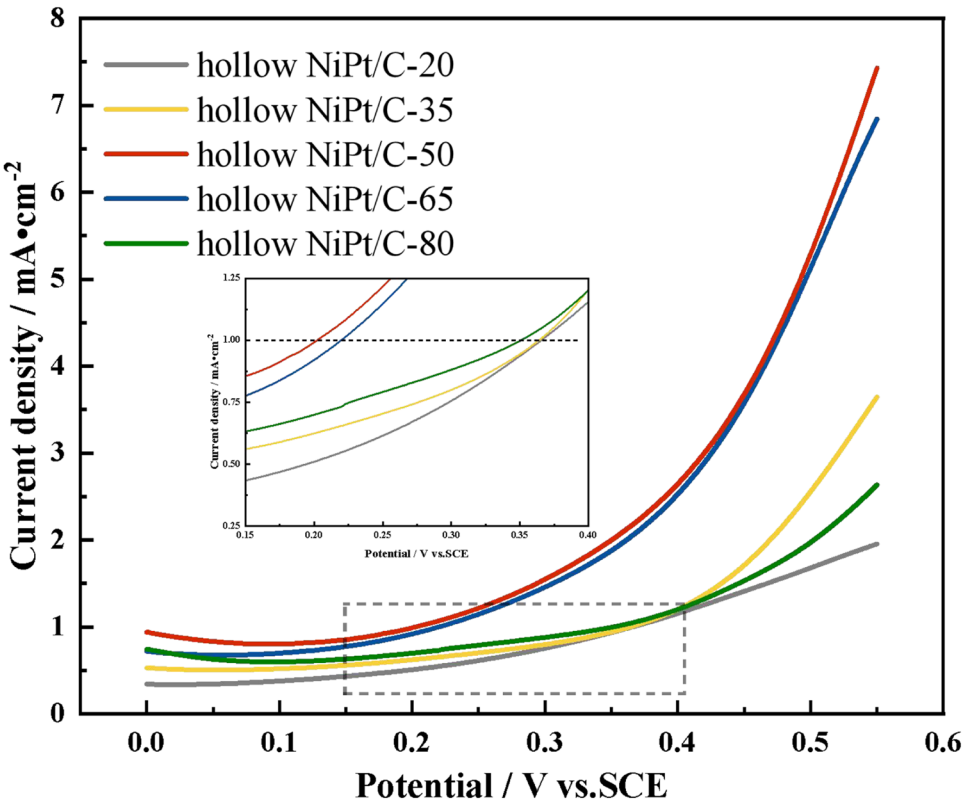

Fig. 5 Linear sweep voltammetry of hollow NiPt/C-20, hollow NiPt/C-35, hollow NiPt/C-50, hollow NiPt/C-65, and hollow NiPt/C-80. Lsv curves were tested in 0.5 M H_2SO_4 and 0.5 M CH_3OH. Scan rate 50 $mV{\cdot}s^{-1}$ in nitrogen atmosphere at RT

In order to better explain the reason why it has excellent catalytic activity, the cyclic voltammetric determination of hollow NiPt/C-50 and commercial Pt/C was carried out in N_2-saturated 0.5 M H_2SO_4 solution, and its ECSA was calculated by formula 2–1. ECSA represents the active sites contained in each gram of catalyst (normalized to Pt) in the process of electrocatalytic reaction. The higher the ECSA value, the better the catalytic activity of the catalyst to a certain extent (Fig. 7).

As shown in Fig. 7a and b, the integral area of the hydrogen region of hollow NiPt/C-50 is significantly larger than that of commercial Pt/C. Their electrochemical active area is calculated by the formula, and the results are shown in Fig. 7c. The ECSA of hollow NiPt/C-50 is 56.64 $m^2{\cdot}g_{Pt}^{-1}$, 1.70 times that of commercial Pt/C (33.39 $m^2{\cdot}g_{Pt}^{-1}$). Higher ECSA has a positive effect on improving the performance of the catalyst of low NiPt/C-50. Obviously, at 25 ℃, when the amount of PVP is 50 mg, the synthesis of hollow NiPt/C can expose more active sites, which is beneficial to improve the activity of methanol electro-catalytic oxidation.

In order to judge the catalytic activity and anti-CO poisoning ability of the catalyst, the prepared catalyst was tested by cyclic voltammetry at 50 mV/s in the electrolyte solution of 0.5 M H_2SO_4 and 0.5 M CH_3OH saturated with N_2, and the commercial Pt/C catalyst was tested under the same conditions as the reference group. As shown in Fig. 8a and b, the mass activity of hollowNiPt/C is 6.534A • mg_{Pt}^{-1}, 2.13 times that of commercial Pt/C, indicating that it has good catalytic activity for methanol oxidation. On the other hand, the reverse current peak hollow NiPt/C and commercial Pt/C, which means that hollow NiPt/C will be effectively oxidized during the forward potential scanning process, while in the reverse potential scanning process, fewer CO_{ads} toxic substances will be produced. Therefore, the prepared hollow NiPt/C catalyst has excellent MOR activity and anti-CO poisoning ability.

The mass activity and area activity of the self-made catalyst and the commercial catalyst are compared according to the Pt load of each catalyst and the ECSA calculated previously. The detailed electrochemical parameters are shown in Table 1.

Figure 9 is the broken line diagram (0.6 V) of the current density change of the catalyst after 250 cycles in 0.5 M H_2SO_4 and 0.5 M CH_3OH solutions. It can be seen that the current density of hollow NiPt/C-50 remains 58.88% of the initial current density after 250 cycles, which is much higher than that of commercial Pt/C (28.6%). From the change trend of current density, both catalysts have a very significant decrease in the first 100 cycles, but the current density of hollowNiPt/C-50 remains basically unchanged after 100 cycles. The above experimental results show that hollowNiPt/C-50 has a smaller loss of catalytic activity than commercial Pt/C after 250 cycles of electrochemical scanning, indicating that it has good durability and stability.

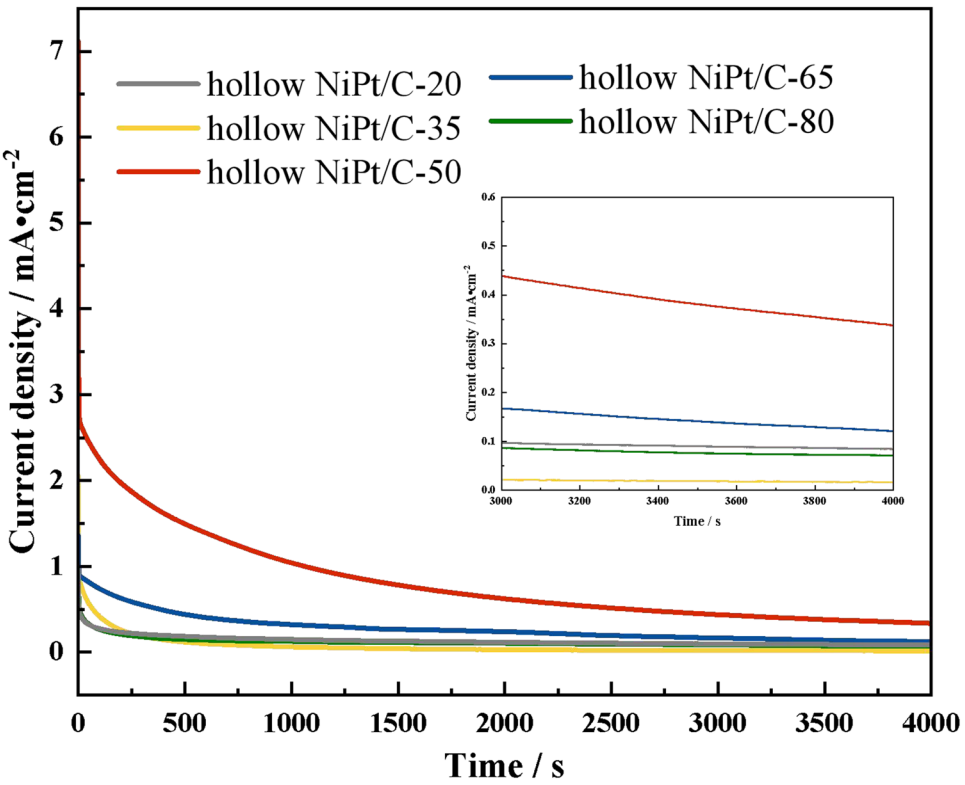

Fig. 6 Chronoamperometry of hollow NiPt/C-20, hollow NiPt/C-35, hollow NiPt/C-50, hollow NiPt/C-65, and hollow NiPt/C-80. CA curves were tested in 0.5 M H_2SO_4 and 0.5 M CH_3OH

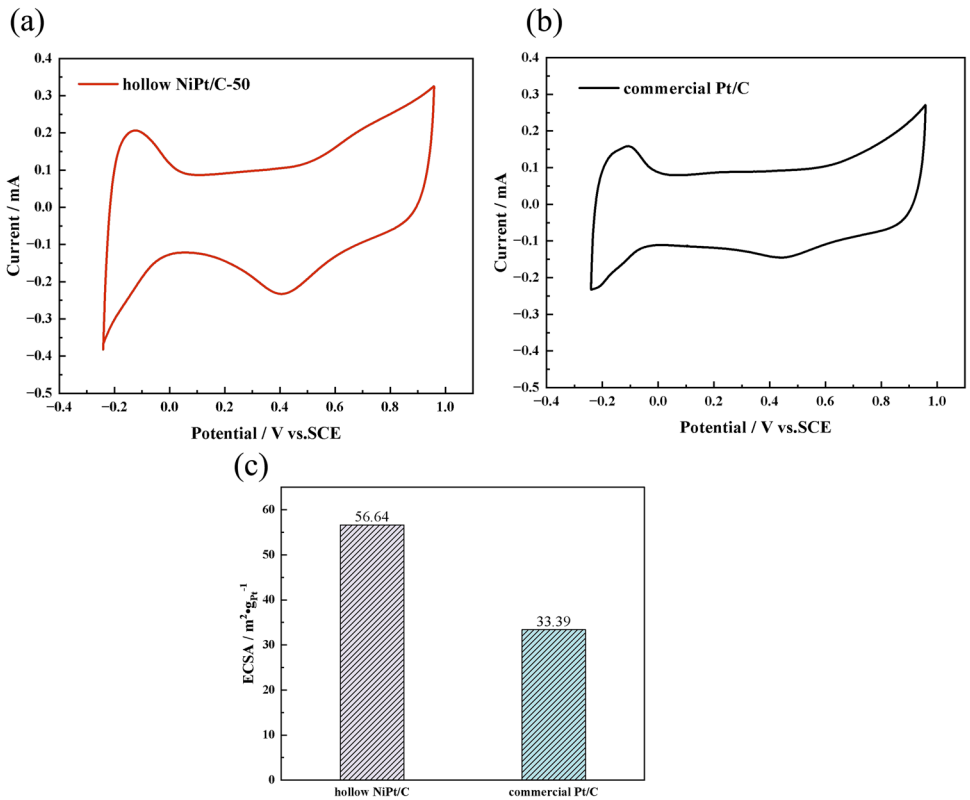

Fig. 7 Cyclic voltammetry results of hollow NiPt/C (**a**) and commercial Pt/C (**b**) in 0.5 M H_2SO_4. The normalized ECSAs of hollow NiPt/C and commercial Pt/C(c). Scan rate 50 $mV{\cdot}s^{-1}$ in nitrogen atmosphere at RT

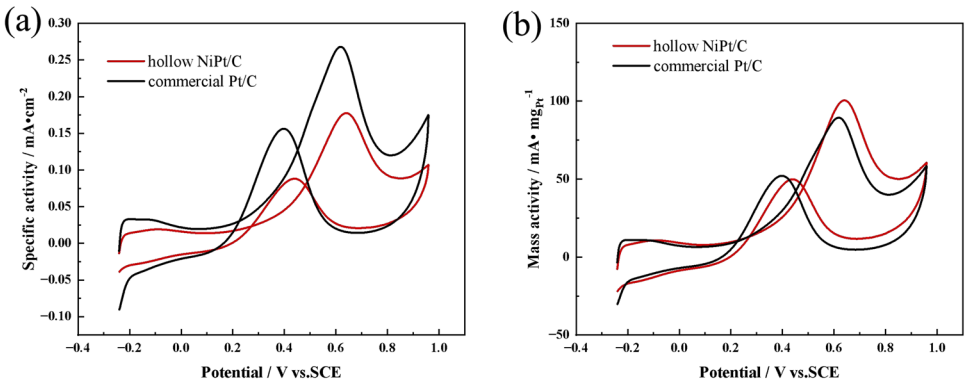

Fig. 8 Cyclic voltammetric results of hollow NiPt/C (**a**) and commercial Pt/C (**b**) in 0.5 M H_2SO_4

The surface electronic structures of the binary hollow NiPt/C samples and the chemical state characterization of Pt and Ni are shown in Fig. 10. According to XPS full-spectrum analysis, binding energy signals of Pt, Ni, and C elements were detected on the hollow NiPt/C surface. It is laterally proven that Ni in the hollow NiPt/C sample can be retained on the surface or near the surface of the material, consistent with the EDS element surface scanning test results. Compared with the EDS results, the content of Ni in the samples decreased significantly, indicating that the surfaces of the two samples were rich in Pt. As shown in Figs. 10b, both Pt4f5/2 and 4f7/2 binding energy peaks can be deconvoluted to form two adjacent binding energy peaks, representing the zero and divalent states of Pt, respectively, and the surface is dominated by the zero valence state Pt(0).

The Pt4f5/2 and 4f7/2 binding energies of binary hollow NiPt/C are between 74.90 and 71.61 eV, respectively. Compared with pure Pt, the shift towards a higher energy direction indicates that the d band center of the Pt atom moves downward. This may be due to the introduction of Ni, which modifies the electronic structure of Pt on the surface of the binary hollow NiPt/C sample. Some studies have shown that the downward deviation of the center of the d band of the surface atoms of the catalyst from the Fermi level can lead to a decrease in the binding energy of the catalyst surface to the catalytic reaction intermediate, leading to an accelerated desorption process for the intermediate, directly leading to a faster catalytic reaction kinetic process, and a corresponding increase in the activity of the catalyst. Figure 10d shows the Ni2p binding energy spectra of the two samples. According to the peak splitting results, the four Ni2p binding energy peaks of the sample are Ni (852.25 eV and 868.14 eV) and NiO (856.4. eV and 874.26 eV), respectively. It can be inferred that the catalytic surface Ni is dominated by the divalent oxidation state. However, the Ni characteristic peak of this sample is not very obvious, indicating that most of the Ni templates were involved in the reaction during the preparation process, and very little Ni remained in the sample.

Table 1 Electrochemical performance parameters of various catalyst electrodes

Catalyst	$I_{p,f}/I_{p,b}$	Specific activity (mA• cm^{-2})	Mass activity (mA• mg$_{Pt}^{-1}$)	ECSA ($m^2 \cdot g^{-1}$)
Hollow NiPt/C	2.01	0.177	100.48	56.64
Commercial Pt/C	1.74	0.266	89.46	33.39

Conclusion

In conclusion, we synthesized a series of hollow Pt-Ni nanocatalysts supported by XC-72 with different PVP dosages by the current displacement method. The nanocatalyst was characterized by transmission electron microscopy (TEM) and X-ray diffraction (XRD). The

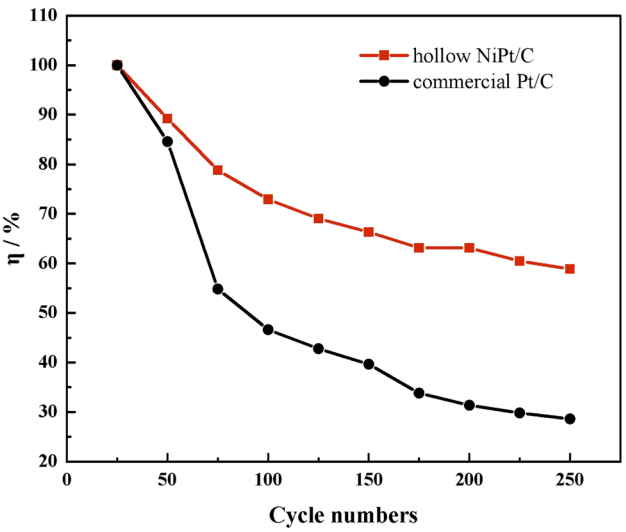

Fig. 9 Cyclic voltammetry circulating for 250 cycles results of hollow NiPt/C (**a**) and commercial Pt/C (**b**) in 0.5 M H_2SO_4 and 0.5 M CH_3OH. Line chart of current density change during cycle (**c**). Scan rate 50 mV·s^{-1} in nitrogen atmosphere at RT

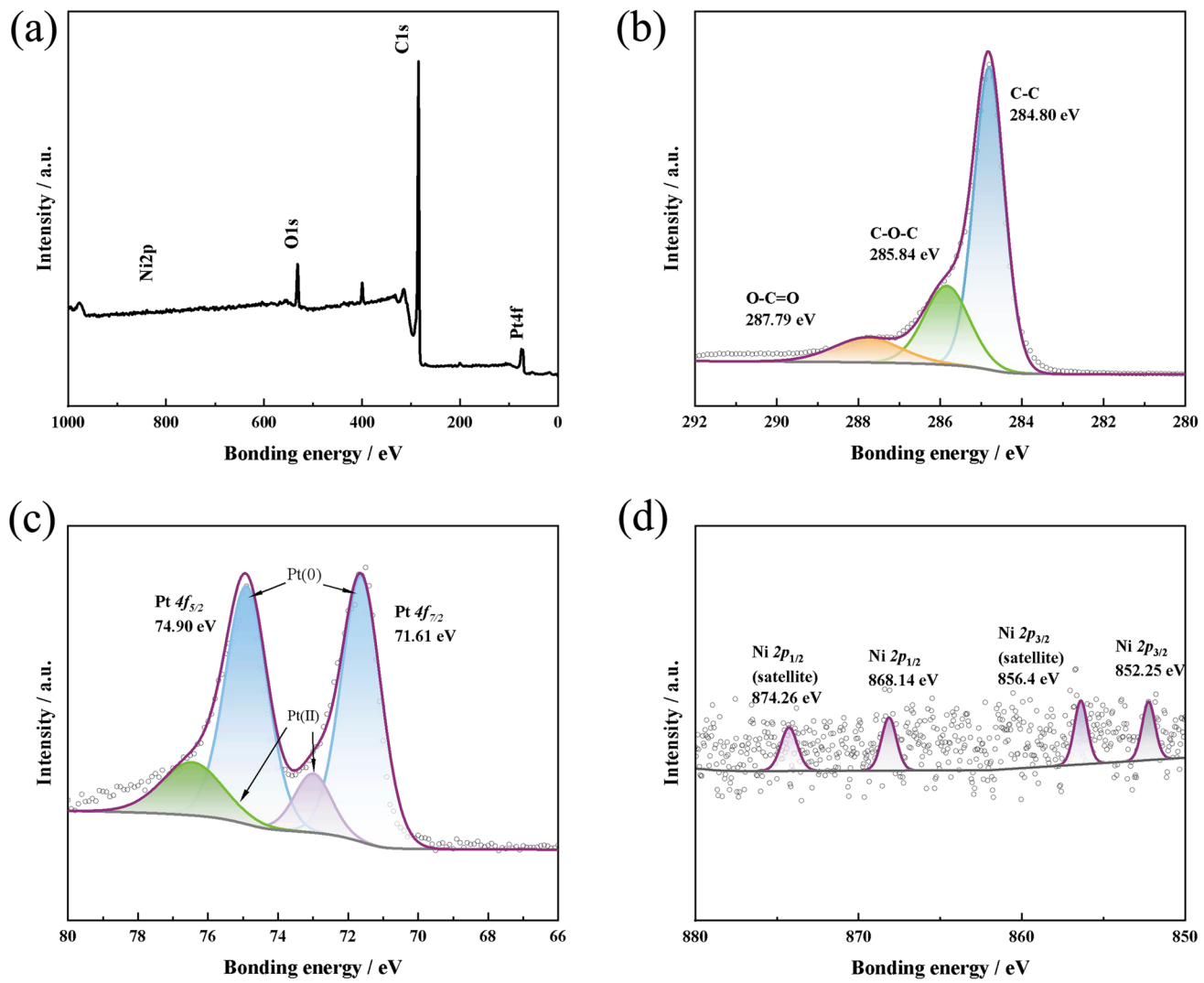

Fig. 10 XPS spectra of the full spectrum (**a**), C 1 s (**b**), Pt 4f (**c**). and Ni 2p (**d**) for hollow NiPt/C samples

shell of the nanocatalyst is composed of many 1 ~ 2-nm Pt particles, and contains more (111) crystal planes. In theory, it has good resistance to methanol poisoning. Through electrochemical tests, the catalyst with the best performance was selected as the catalyst synthesized at the dosage of 50-mg PVP. The electrocatalytic performance of nanocatalysts for methanol oxidation was evaluated by voltammetry. It was found that compared with hollow NiPt/C and commercial Pt/C nanocatalysts, nanocatalysts showed excellent electrocatalytic ability, high electrochemical active surface area (ECSA), and good toxicity resistance. The enhanced catalytic activity of hollow NiPt/C nanocatalysts is probably due to the unique hollow structure and the synergistic effect of Pt and Ni in the catalyst. In addition, the large surface area, high conductivity, and good stability of graphene are also conducive to improving the electrocatalytic performance of the prepared nanocatalyst. The prepared nanocatalyst will find potential applications in fuel cells due to its good electrocatalytic properties. This work has opened up a new way for the design of platinum-based bimetallic nanocatalysts with novel structures.

Acknowledgements The authors are thankful for the support provided by School of Marine Science and Technology, Harbin Institute of Technology, Weihai.

References

1. Zuo Y, Sheng W, Tao W et al (2022) Direct methanol fuel cells system–a review of dual-role electrocatalysts for oxygen reduction and methanol oxidation. J Mater Sci Technol 114:29–41

2. Ramli Z, Kamarudin SK (2018) Platinum-based catalysts on various carbon supports and conducting polymers for direct methanol fuel cell applications: a review. Nano Scale Res Lett 133:13551–13557
3. Zhou X, Gan Y, Du J et al (2013) A review of hollow Pt-based nanocatalysts applied in proton exchange membrane fuel cells. J Power Sources 232:310–322
4. Guo XJ, Zhang Q, Li YN et al (2022) Nanosized Rh grown on single-walled carbon nanohorns for efficient methanol oxidation reaction. Rare Met 41:2108–2117
5. Brouzgou A, Song SQ, Tsiakaras P (2012) Low and non-platinum electrocatalysts for PEMFCs: current status, challenges and prospects. Appl Catal B 127:371–388
6. Othman R, Dicks AL, Zhu Z (2012) Non precious metal catalysts for the PEM fuel cell cathode. Int J Hydrog Energy 37(1):357–372
7. Ishihara A, Ohgi Y, Matsuzawa K et al (2010) Progress in non-precious metal oxide-based cathode for polymer electrolyte fuel cells. Electrochim Acta 55(27):8005–8012
8. Baronia R, Goel J, Tiwari S et al (2017) Efficient electro-oxidation of methanol using PtCo nanocatalysts supported reduced graphene oxide matrix as anode for DMFC. Int J Hydrog Energy 1042(15):10238–10247
9. Guerrero-Ortega LPA, Manzo-Robledo A, Ramirez-Meneses E et al (2018) Methanol electro-oxidation reaction at the interface of (bi)-metallic (PtNi) synthesized nanoparticles supported on carbon Vulcan. Int J Hydrog Energy 43(12):6117–6130
10. Zhang J, Sun S, Li Y et al (2017) A strategy in deep eutectic solvents for carbon nanotube-supported PtCo nanocatalysts with enhanced performance toward methanol electrooxidation. Int J Hydrog Energy 42(43):26744–26751
11. Liu Y, Ren G, Wang M et al (2019) Facile synthesis of trimetallic PtAuCu alloy nanowires as high-performance electrocatalysts for methanol oxidation reaction. J Alloy 780:504–511
12. Chen J, Lim S, Kuo C et al (2019) Sub-1 nm PtSn ultrathin sheet as an extraordinary electrocatalyst for methanol and ethanol oxidation reactions. J Colloid Interface 545:54–62
13. Khan TS, Jalid F, Haider MA (2018) First-principle microkinetic modeling of ethanol dehydrogenation on metal catalyst surfaces in non-oxidative environment: design of bimetallic alloys. Top Catal 61(18–19):1820–1831
14. Lu Q, Huang J, Han C et al (2018) Facile synthesis of composition-tunable PtRh nanosponges for methanol oxidation reaction. Electrochim Acta 266:305–311
15. Bin Yousaf A, Imran M, Kasak P et al (2017) Enhanced and durable electrocatalytic performance of thin layer PtRu bimetallic alloys on Pd-nanocubes for methanol oxidation reactions. Catal Sci Technol 7(15):3283–3290
16. Yin JW, Wang J, Ma YB et al (2021) Recent advances in the controlled synthesis and catalytic applications of two-dimensional rhodium nanomaterials. Acs Mater Lett 3(1):121–133
17. Huang HJ, Wei YJ, Yang Y et al (2021) Controllable synthesis of grain boundary-enriched Pt nanoworms decorated on graphitic carbon nanosheets for ultrahigh methanol oxidation catalytic activity. J Energy Chem 57:601–609
18. Wu B, Du F, Wang H et al (2022) Effects of annealing temperature of PtCu/MWCNT catalysts on their electrocatalytic performance of electrooxidation of methanol. Ionics 28(1):369–382
19. Zheng F, Liu S, Kuo C (2016) Ultralow Pt amount of Pt-Fe alloys supported on ordered mesoporous carbons with excellent methanol tolerance during oxygen reduction reaction. Int J Hydrog Energy 41(4):2487–2497
20. Ma X, Luo L, Zhu L et al (2013) Pt-Fe catalyst nanoparticles supported on single-wall carbon nanotubes: direct synthesis and electrochemical performance for methanol oxidation. J Power Sources 241:274–280
21. Liu H, Yang D, Bao Y, et al (2019) One-step efficiently coupling ultrafine Pt-Ni_2P nanoparticles as robust catalysts for methanol and ethanol electro-oxidation in fuel cells reaction. J Power Sources 434:226754.1–226754.9
22. Stamenkovic VR, Fowler B, Mun BS et al (2007) Improved oxygen reduction activity on Pt3Ni(111) via increased surface site availability. Science (New York, N.Y.) 315(5811):493–497
23. Huang X, Zhu E, Chen Y et al (2013) A facile strategy to Pt3Ni nanocrystals with highly porous features as an enhanced oxygen reduction reaction Catalyst. Adv Mater 25(21):2974–2979
24. Yuan X, Jiang X, Cao M et al (2019) Intermetallic PtBi core/ultrathin Pt shell nanoplates for efficient and stable methanol and ethanol electro-oxidization. Nano Res 12(2):429–436
25. Bu L, Zhang N, Guo S et al (2016) Biaxially strained PtPb/Pt core/shell nanoplate boosts oxygen reduction catalysis. Science 354(6318):1410–1414
26. Sevilla M, Sanchis C, Valdes-Solis T et al (2009) Highly dispersed platinum nanoparticles on carbon nanocoils and their electrocatalytic performance for fuel cell reactions. Electrochim Acta 54(8):2234–2238
27. Xia Z, Guo S (2019) Strain engineering of metal-based nanomaterials for energy electrocatalysis. Chem Soc Rev 48(12):3265–3278
28. Meng W, He H Y, Yang L, et al (2022) 1D-2D hybridization: nanoarchitectonics for grain boundary-rich platinum nanowires coupled with MXene nanosheets as efficient methanol oxidation electrocatalysts Chem Eng J 450(30):137932
29. Shan A, Chen Z, Li B et al (2015) Monodispersed, ultrathin NiPt hollow nanospheres with tunable diameter and composition via a green chemical synthesis. J Mater Chem A 3(3):1031–1036
30. Sun Q, Ren Z, Wang R et al (2011) Platinum catalyzed growth of NiPt hollow spheres with an ultrathin shell. J Mater Chem 21(6):1925–1930
31. Hu Y, Wu P, Zhang H et al (2012) Synthesis of graphene-supported hollow Pt-Ni nanocatalysts for highly active electrocatalysis toward the methanol oxidation reaction. Electrochim Acta 85:314–321
32. Wu J, Yang H (2012) Study of the durability of faceted Pt3Ni oxygen-reduction electrocatalysts. Chem Cat Chem 4(10):1572–1577
33. Zhang H, Yin Y, Hu Y et al (2010) Pd@Pt core-shell nanostructures with controllable composition synthesized by a microwave method and their enhanced electrocatalytic activity toward oxygen reduction and methanol oxidation. J Phys Chem C 114(27):11861–11867
34. Zhang X, Zhang J, Huang H et al (2017) Platinum nanoparticles anchored on grapheneoxide-dispersed pristine carbon nanotube supports: high-performance electrocatalysts towardmethanol electrooxidation. Electrochim Acta 258:919–926